Dalton Transactions

Sulfur Functionalized Biocarbon Sorbents for Low-Concentration Mercury Isolation

Journal:	*Dalton Transactions*
Manuscript ID	DT-ART-08-2023-002625.R1
Article Type:	Paper
Date Submitted by the Author:	30-Oct-2023
Complete List of Authors:	Austin Jr, Douglas; Delaware State University, Chemistry; Delaware State University Kousar, Jahan; Delaware State University Feng, Xu; University of Delaware Carney, Jared; Delaware State University Hensley, Dale; Oak Ridge National Laboratory, Nanophase Materials Sciences Chen, Jihua; Oak Ridge National Laboratory, Center for Nanophase Materials Sciences Altidor , Brianna ; Delaware State University Guo, Zhiyong; Fuzhou University, Materials Science and Engineering Michaelis, Elizabeth; Delaware State University Kebaso, Mariana ; Delaware State University Yue, Yanfeng; Delaware State University, Department of Chemistry

Journal Name Dalton Transactions Dynamic Article Links ▶

Cite this: DOI: 10.1039/c0xx00000x

www.rsc.org/xxxxxx

ARTICLE TYPE

Sulfur Functionalized Biocarbon Sorbents for Low-Concentration Mercury Isolation

Douglas Austin,[a] Kousar Jahan,[a] Xu Feng,[b] Jared Carney,[a] Dale K. Hensley,[c] Jihua Chen,[c] Brianna E Altidor,[a] Zhiyong Guo,[d,*] Elizabeth Michaelis,[a] Mariana K Kebaso,[a] Yanfeng Yue,[a,*]

Received (in XXX, XXX) Xth XXXXXXXXX 20XX, Accepted Xth XXXXXXXXX 20XX
DOI: 10.1039/b000000x

Sulfur functionalized biocarbons were prepared from naturally abundant lignin alkali with sodium thiocyanate as an activation agent and a sulfur source. The resultant biocarbon sorbents showed a high mercury isolation ability from aqueous solutions, where high surface area and doping of sulfur paramountly aids the uptake of mercury, i.e., 0.05 g of biocarbon sorbent removed 99% of mercury from 250 mL simulated wastewater with an initial concentration of mercury of 10 mg·L^{-1}.

1. Introduction

In recent years, many studies have been devoted to mitigating environmental pollution.[1] The study of toxic heavy metals and their impact on the environment and subsequently determine to mitigate environmental pollution.[2] The term 'heavy metal' refers to any metal and metalloid element with a relatively high molecular weight 63.5–200.6 g mol^{-1} and densities higher than density ranging from 5 g cm^{-3} and are toxic or poisonous when the concentrations reach a specific limit.[3] Usually, the heavy metals include mercury (Hg), cadmium (Cd), arsenic (As), chromium (Cr), thallium (Tl), zinc (Zn), nickel (Ni), copper (Cu), and lead (Pb).[4] Among them, mercury is studied intensely because of its high toxicity due to its bioaccumulation and biomagnification.[5] Mercury is one of the few heavy metals biomagnified along the food chain and can be carried from environmental contamination to human consumption.[6-20]

Many methods have been utilized to remove heavy metals like mercury from water, including ion exchange, membrane filtration, chemical precipitation, photocatalytic reaction, and adsorption. Many of the techniques previously mentioned are limited by high cost, complex treatment possibility of secondary pollution, and high energy needs.[21] In contrast, activated carbon used as a sorbent is a cost efficient method for removing heavy metals from water.[22] Activated carbon sythisized from lignocellulosic material is also very well-suited for environmental applications because of its low toxicity.[23] The primary components of plant lignocellulosic biomass are cellulose, hemicellulose, and lignin. Lignin, due to its abundance, various functional groups such as methoxy, phenolic and aliphatic hydroxyl, carbonyl, and desirable properties like higher carbon content, degradability, renewability, safety, and cost effectiveness, stands out as a remarkably versatile material.[24] On a global scale, the annual production of different forms of lignin, such as kraft lignin, alkaline lignin, and sodium lignosulfonate, ranges from 500 to 3,600 million tones,[25] mostly as a by-product

of the paper-making and biorefinery industries. It serves as a sustainable source of biobased materials with the potential to be transformed into a range of value-added carbon products with tunable morphology, pore size, crystallinity and surface functionality through tailored pretreatments and manufacturing techniques. Because of its high carbon content and aromatic groups, lignin produces substantially more solid char than other biomass sources, making it a cost-effective choice. Activated carbon is a carbon-rich material with a porous structure, high surface area, and pore volume. Due to these properties, activated carbons have been used for gas storage and separation, solvent recovery, catalyst/catalyst support, contaminant removal, and wastewater treatment.[26] Activated carbon has garnered much attention and research studies as electrodes for energy storage devices.[27] Activated carbons are achieved through the carbonization of carbon precursors. Most non-carbon elements such as oxygen, nitrogen, and hydrogen are eliminated as a gas through pyrolytic decomposition in the presence of activation reagents, including bases, salts, and even gases.[28] The efficiency of activated carbon for removing ions such as mercury depends on surface chemistry, a developed pore structure, and a high surface area.[29] It has been studied that doping with heteroatoms could introduce more active sites into carbon-based materials.[30] Researchers have studied sulfur as a functional group to utilize it for mercury remediation. Sulfur complexes bonded on the carbon surface have good stability and can resist extraction by solvent and decomposition at temperatures up to 1000° C.[31] Sulfur is usually introduced to the surface of activated carbon in an inert atmosphere with a sulfurizing agent. Common sulfurizing agents include elemental S, CS_2 dimethyl disulfide, SO_2, and Na_2S. These sulfurizing agents form many sulfur groups on the surface of the carbon, including; C−S, S−S, S=O, S_8 rings, S_n chains, sulfoxides, thiophenes, or sulfone groups (Scheme 1).[32] Due to the larger atom size of sulfur than carbon, sulfur molecules extend beyond the graphene plane, contributing unique properties to the host carbon. Sulfur functionality on the surface includes increased reactivity, increased induced polarizability.[33] The preparation of sulfur-functionalized activated carbons with sulfur heteroatoms can increase the affinity of the sulfurized carbons towards heavy metals. The order is Hg(II) > Pb(II) > Cd(II) > Ni(II) at a pH of 7 or greater. It has been studied that thiolate groups can create strong complexes with Hg^{2+} with logK >> 14.[34] The use of sulfur groups sulfur and mercury form mercuric sulfide on the surface of the carbon, based on hard-soft acid-base theory. Mercuric sulfide is a less harmful form of mercury due to its insolubility and very low volatility.[35] It is theorized that mercury cations prefer to bind with sulfur based groups over oxygen even though they are plentiful and readily available on the surface of activated carbon. This gives rise to the theory hypothesis that by increasing sulfur content in a material, the mercury uptake should be more efficient.[36]

2. Experimental

2.1 Materials

Lignin alkali, hydrochloric acid, and isopropyl alcohol were obtained from Millipore Sigma and used as received. Sodium thiocyanate, sodium citrate, citric acid, and Spex CertiPrep gold standard (100 mg·L^{-1}) were obtained from Fischer Scientific and used as received.

2.2 Synthesis of sulfur functionalized biocarbons

Here we report the synthesis of sulfur functionalized mesoporous bio-carbon sorbent material using lignin alkali as a carbon source and sodium thiocyanate as a sulfur source. Sulfur groups were grafted onto an inert, high surface area activated carbon substrate. Because of its high carbon content, lignin alkali was used as a precursor. Four activated biocarbon were synthesized: biocarbon

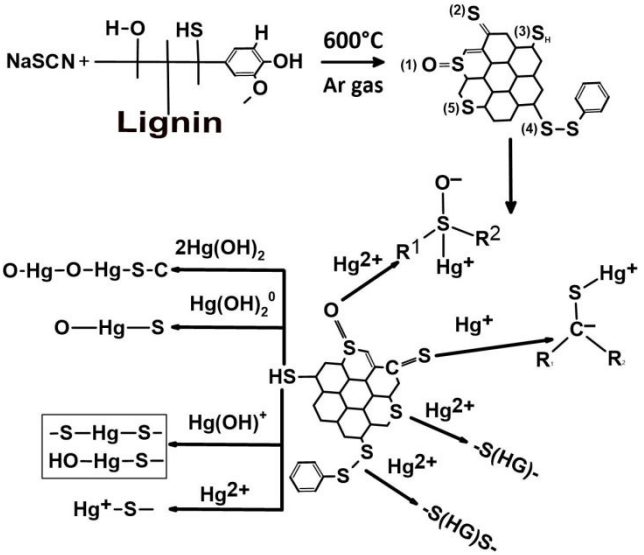

Scheme 1. Schematic diagram of sulfur functionalized biocarbon. Possible sulfur functionalities on carbon surface; (1) Sulfone, (2) thioketone, (3) thiol, (4) thioether, (5) carbon sulfur bridge within the graphene plane.

made from pristine lignin alkali (2.0 g) without anyactivation agent denoted Ligsulf-0 and three other biocarbon synthesized from 1.0 g of lignin alkali and desired amount of NaSCN, with a mass ratio of lignin alkali and NaSCN as 1:1, 1:2, and 1:3 were denoted as Ligsulf-1/1, Ligsulf-1/2, and Ligsulf-1/3, respectively. These samples were uniformly mixed and ground in a ceramic mortar. Then the mixture was transferred to a quartz boat for use in a tube furnace. Both pyrolysis and activation were conducted simultaneously in a 1-inch quartz tube sealed and then filled with argon gas to produce an inert atmosphere. The tube furnace was set to ramp up from ambient temperatures to 250 °C at a rate of 5 °C/min, sustaining at 250 °C for two hours. The tube furnace then ramped to 600 °C at a rate of 5 °C/min, which sustained at 600 °C for another two hours. Once the functionalized biocarbon product was cooled to room temperature, it was ground into powder and washed with 1M HCl for 24 hours. Next, the acid was decanted, and the biocarbon was washed with water and the Isopropyl alcohol. Lastly, the biocarbon was dried in a vacuum oven at 110 °C for 24 hours. The nitrogen adsorption tests were conducted for porosity screening.

2.3 Characterizations

The sulfur functionalized biocarbon's phase purity was identified using a Rigaku MiniFlex 600 X-ray diffractometer (Cu-K radiation, λ = 1.5418 Å). Scanning electron microscopy (SEM, Quanta FEG 250) and an energy-dispersive detector (Oxford X-

MaxN EDS) detected the samples' microstructure, surface morphology features, and elemental analysis. Analysis of graphitization degree of biocarbon after carbonization by Horiba Xplora Plus Raman measurements (Ar+ laser, λ = 532 nm). Nitrogen adsorption-desorption studies determined carbon products' specific surface area and pore size distribution (Quantachrome NOVA 4200e) at 77 K. The samples were degassed for 6 hrs at 200 °C under flowing nitrogen. Elemental analysis was done by CHNS Elmentar Analyzer. XPS was performed on a Thermo Scientific K-Alpha+ XPS system (Thermo Fisher Scientific Inc., Waltham, MA, USA) equipped with a monochromatic Al K-alpha X-ray source. High-resolution XPS spectra were acquired with a 400 µm X-ray beam and a pass energy of 50 eV. The contact angles of the samples with water were tested at room temperature using an Osilla Contact Angle Goniometer. The surface functional groups were obtained using Agilent Cary 630 Fourier transform infrared spectrometer (FTIR) with Attenuated total reflectance (ATR) accessory.

2.4 Mercury adsorption tests

The dried sorbent (0.05 g) was allowed to equilibrate respectively with 250 mL of simulated mercury contaminated water composed of sodium citrate (24.269 g, 0.0825 M), citric acid (3.358 g, 0.0175 M) and mercuric chloride (0.0135g, 0.034 mM) in ultrapure water. Citric acid and sodium citrate were used to create a buffer solution for this research. The final pH of the solution was 6.03. The sorbent was dispersed in the stock solution in an Erlenmeyer flask and shaken for 48 hours at 22 °C, followed by filtration of the supernatants. The amount of metal ion uptake was determined from the concentration difference between the test's beginning and end. The amount of mercury adsorbed by the sample was calculated using **Equation 1** where q_e is the mercury uptake by the sorbent under equilibrium condition (mg/g); C_0 and C_e are the initial and final concentrations of mercury (mg/L); V is the volume of the stock solution, and m is the mass of the sorbent used.

Eq. (1)

Mercury concentrations were determined using an Agilent 7900 inductively coupled plasma mass spectrometer (ICP-MS). Samples were aspirated at 100 µL min^{-1} with a Teflon SP nebulizer connected to a quartz spray chamber. Internal standards containing Li, Bi, Ho, In, Sc, Tb, and Y were added via an online injection port. Mercury was quantified against a 5-point calibration curve using the average of three replicate measurements per sample. Semi-quantitative full mass range survey scans were collected prior to sample analysis. Instrument washout was monitored between samples. When analyzing Hg with ICP-MS, Hg ions can be lost due to volatilization and adsorption on components used to store and transport samples during analysis.[37] To prevent this volatility, gold in the form of a gold solution in 5 % v/v HNO_3 can be used as a stabilizing and preserving agent.[38] HCl is an ideal acid for the analysis of Hg using ICP-MS in the presence of gold for stabilization (**Table 1**). One plausible mechanism for gold and hydrochloric acid's mercury stabilizing action is that they prevent undesirable Hg^{2+} reduction (**Equation 2**). This can be explained by Au^{3+} being a strong oxidizing agent compared to mercury (**Equation 3**) which helps keep Hg^{2+} in the solution. The presence of HCl provides a chloride ligand to mercury forming tetrachord mercuric(II) (**Equation 4**), which has a lower reduction potential than Hg^{2+}, limiting the formation of Hg^0. Also, in solution, the formation of $HgCl_4^{2-}$, is expected to prevent the absorption of mercury on polypropylene, a common plastic used in analytical analysis and chemical storage.[39] The recommended concentration of gold is 1 ppm.[40] The ability to measure mercury concentration in aqueous solutions is vital to understanding the effect of mercury remediation techniques. It has been studied that mercury has a very low vapor pressure and can be easily lost.[41] It has been reported that mercury can be lost from both polyethylene and glass containers when mixed with distilled water, if not stabilized with a preserving agent.[37] Adsorption tests were also performed in the presence of competitive ions; Ca^+ and Na^+. Removal efficiency did not change in the presence of these ions.

Table 1. Redox potentials of mercury in the presence of either hydrochloric acid or Au^{3+}.

$Hg^{2+} + 2e^- \rightarrow Hg$	$E^0 = 0.85$	*Eq. (2)*
$AuCl_4^- + 3e^- \leftrightarrow Au + 4Cl^-$	$E^0 = 1$	*Eq. (3)*
$[HgCl_4]^{2-} + 2e^- \leftrightarrow Hg^0 + 4Cl^-$	$E^0 = 0.41$	*Eq. (4)*

3. Results and discussion

Table 2. Porosity of sulfur functionalized biocarbon sorbents.

Sample	Surface area ($m^2 \cdot g^{-1}$)	Pore volume ($cc \cdot g^{-1}$)	Pore diameter (Å)
Ligsulf-0	6.2	0.00133	7.713
Ligsulf-1/1	1084.0	0.586	7.374
Ligsulf-1/2	1413.0	0.792	7.049
Ligsulf-1/3	716.6	0.382	1.475

3.1 Properties of sulfur functionalized activated biocarbons

The specific surface area of the sulfur functionalized biocarbon was determined by N_2 adsorption–desorption measurement. According to IUPAC classifications, nitrogen adsorption-desorption plots of all biocarbon materials show a type I isotherm as seen in **Figure 1**. The as prepared Ligsulf-1/2 had a surface area of 1413 $m^2 \cdot g^{-1}$, with a total pore volume of 7.9 $cc \cdot g^{-1}$ (**Table 2**). The addition of sulfur increased the surface area significantly compared to the unmodified carbon (6.2 $m^2 \cdot g^{-1}$) and Ligsulf-1/1 (1084 $m^2 \cdot g^{-1}$). The rapidly increasing adsorption volume at very low relative pressure indicates the presence of micropores in these biocarbon. The second uptake at high relative pressure is due to the textural meso/macropores formed by packing the nanosized particles (**Figure 1**). A narrow pore size distribution was observed with pore diameter of micropore centred at ca. 1.5-1.8 nm for samples Ligsulf-1/1, Ligsulf-1/2, and Ligsulf-1/3 (**Figure S1**). Abundant porosity in sample lead to an increase in a high surface area as well as a fast mercury uptake (**Table 3**). Wettability studies showed that sulfur functionalization increased hydrophilicity. In the absence of sulfur doping ligsulf-0 displayed hydrophobic properties. Hydrophilicity increased ligsulf-0<ligsulf-1/1<ligsulf-1/2. Ligsulf-1/3 was slightly more hydrophobic, this could be due to the decrease in surface area (Figure S2).[42] CNHS Elemental Analyzer determined the dopped S components in the resultant biocarbon. The sample Ligsulf-1/2 showed a sulfur content of 6% (**Table S1**). With the abundance of hierarchical pores, the adsorbate may enter channels formed in the material allowing for more effective uptake in mercury ions for fast mass transfer.[43] These results match with previous studies that hierarchical porosity

benefit from the contaminant uptake due to fast kinetic adsorption.[44,45] ATR-FTIR was used to study the surface chemistry of the sulfur functionalized sorbents at different ratios and after absorbance of mercury. There was no discernible difference in the FTIR spectrogram. The surface chemical composition of the lignin-derived biocarbon (Ligsulf-0) and sodium thiocyanate-functionalized biocarbon (Ligsulf-1/2) was analyzed by X-ray photoelectron spectroscopy. As shown in **Figure 2A**, the XPS survey spectra of both samples exhibited the peaks corresponded to C, O, N, and S; however, the intensity of these peaks varied. The sulfur content in the Ligsulf-0 attributed to the presence of sulfur in the raw alkali lignin, as shown in scheme 1. The high-resolution S 2p XPS spectra of both the samples were deconvoluted to study the detailed chemical states of sulfur moieties present on the adsorbent (**Figure 2B, C**). The signals in the S 2p spectra were deconvoluted into four peaks at around 163.58, 164.6 eV and 167.68, 169.08 eV confirmed the presence of C-S bonds and ($C-SO_n-C$) oxidized sulfur or sulfone functional groups. [46,47] The notable increase in different peaks of S 2p indicates the high proportion of C–S bonds and oxidized sulfur moieties in the sodium thiocyanate modified biocarbon. Oxidized sulfur peaks were more prominent in the later one. Similarly, C 1s, O 1s and N 1s spectra further deconvoluted into different peaks and results are shown in supporting information (Figure S3).

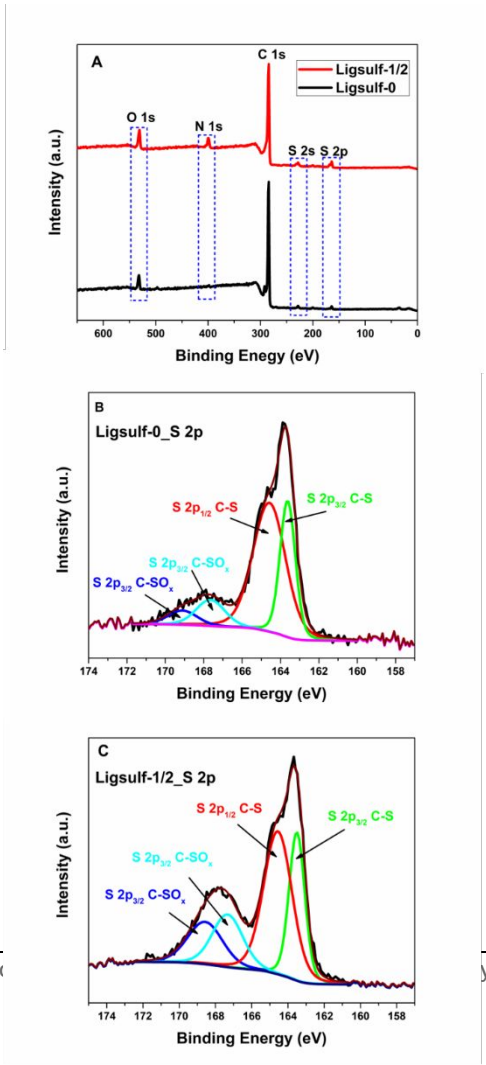

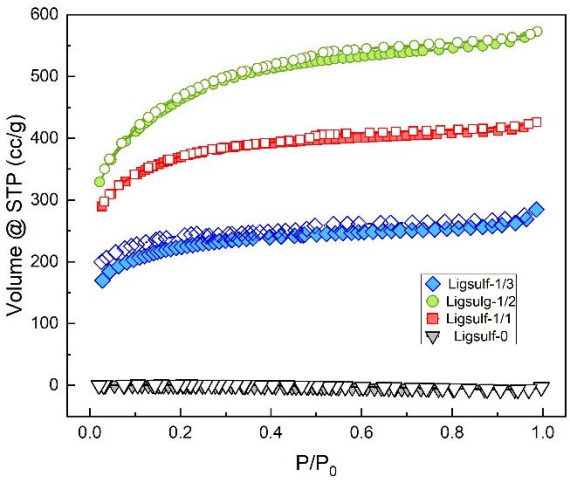

Figure 1. N_2 adsorption isotherms for the carbon sorbents.

Figure 2. Surface composition analysis of as prepared Ligsulf-0 and Ligsulf-1/2; XPS survey spectra of Ligsulf-0 and Ligsulf-1/2 (A); High resolution S 2p XPS spectra of Ligsulf-0 and Ligsulf-1/2, (B, C).

Scanning electron microscopy (SEM) and transmission electron microscopy (TEM) characterized the samples' morphology and porous structure. In **Figure 3.** SEM images from this biocarbon showed granular size pieces with the size in a range of 1 µm to 30 µm. TEM imaging mainly showed an amorphous carbon structure with small areas of crystalline structure. Furthermore, powder X-ray diffraction (XRD) patterns confirm the absence of unreacted NaSCN and other impurities (**Figure S4**). At approximately 23° and 42°, two diffraction peaks corresponding to the (002) and (100) crystal facets are seen in amorphous carbon with low crystallinity.[48] To understand the importance of the activation agent in forming micropores, a sample was prepared from lignin in the absence of NaSCN as a control sample and named Ligsulf-0. In contrast to the activated biocarbon materials, sulfur heteroatoms block pores giving rise to a smaller surface area and pore diameter.[49]

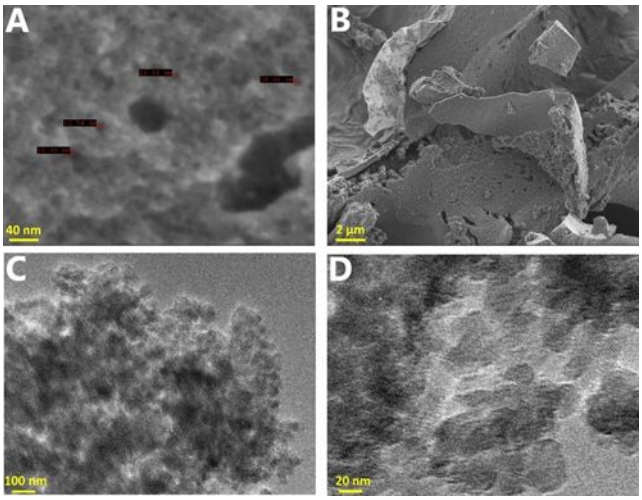

Figure 3. SEM and TEM images of Ligsulf-1/2.

Raman scattering spectra as seen in **Figure 4** demonstrate two broad Raman bands, with the initial peak identified in the range of 1315 cm^{-1}, which can be ascribed to the defect or disordered phase (*D*-band), and the second peak situated at 1601 cm^{-1}, which can be linked to the graphitic phase (*G*-band) of carbon (as shown in **Figure 4**). The *D*-band signifies the vibrations of carbon atoms with a dangling bond in the disordered graphite structure's terminations, while the *G*-band represents the stretching vibration mode of the sp2 hybridized carbon atoms in the graphite layer.[50]

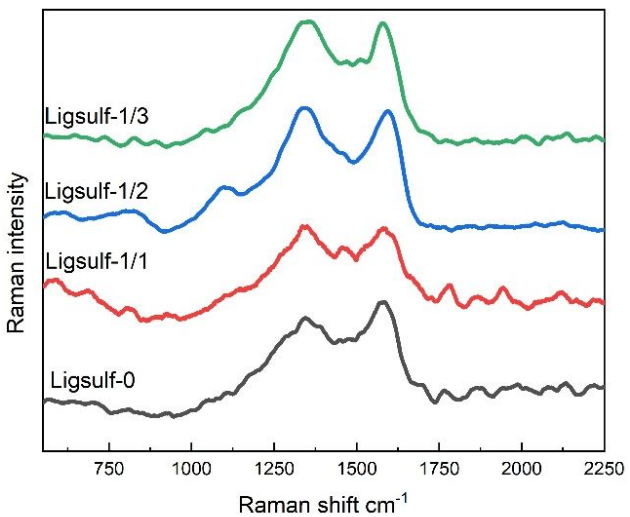

Figure 4. Raman spectra of Ligsulf-0, Ligsulf-1/1, Ligsulf-1/2, and Ligsulf-1/3.

High specific surface area and covalently bound sulfur make these materials ideal candidates as a remediation material for mercury.[45] The biocarbon with the highest surface area was the lead candidate for mercury adsorption, but all products were screened to ensure effectiveness in mercury sequestering. Mercury batch kinetics studies of 4 hours were done to see which biocarbon possessed the most extraordinary adsorption capacity in this study. For this, 0.05 g of Ligsulf-0, Ligsulf-1/1, Ligsulf-1/2, and Ligsulf-1/3 were charged to a flask containing 250 mL of mercury solution concentration of 10 ppm at a pH of 6 and a temperature of 25 °C (**Table 3**).

Table 3. Hg adsorption screening tests for the sulfur functionalized sorbents.

Sample	Initial Concentration ($mg \cdot L^{-1}$)	Final Concentration ($mg \cdot L^{-1}$)	Adsorption Capacity ($mg \cdot g^{-1}$)
Ligsulf-0	10	9.80	1.01
Ligsulf-1/1	10	2.43	37.80
Ligsulf-1/2	10	0.25	48.75
Ligsulf-3/1	10	4.80	26.00

This sulfur functionalized biocarbon was tested under different parameters to evaluate its effectiveness as a mercury adsorbent. As seen in **Figure 5**. initial testing showed a 99 % removal of mercury ions after 24 hours, giving a q_e of 49.8 $mg \cdot g^{-1}$. The biocarbon was further tested under different parameters (**Table 4**) to discover ideal conditions for mercury sequestering.

Table 4. Hg adsorption studies under various conditions.

Temp. (°C)	pH	Mass (g)	Volume ($cc \cdot g^{-1}$)	Final Conc. ($mg \cdot L^{-1}$)	Adsorption capacity ($mg \cdot g^{-1}$)
32	6	0.05	250	0.25	48.75
25	6	0.025	250	3.50	65.00
25	6	0.1	250	[a]	25.00
25	6	0.05	500	[a]	99.98
25	6	0.05	1000	6.34	73.20
25	5	0.05	250	[a]	49.99
25	7	0.05	250	[a]	49.99

Time dependent adsorption kinetics describe how the adsorption process evolves over time.

Additionally, the adsorption process in aqueous solutions is intimately influenced by other experimental parameters, including pH, ionic strength, temperature, solute concentration, sorbent dose, and texture of adsorbents. These parameters affect the adsorption of adsorbate onto any adsorbent. As a result, these parameters must be considered when determining the contact time at which equilibrium is achieved. Initial kinetic studies showed that 97.5 % of mercury ions were adsorbed with the sulfur functionalized biocarbon after 4 hours. Kinetic studies of four hours were initiated with different parameters bearing in mind the initial findings. Ligsulf-1/2 performed well within the 6–8 pH range. To better understand the mercury adsorption mechanism, pseudo-first-order,

Table 5. A comparison of Hg(II) removal with sulfur functionalized sorbents.

Sample	Precursor	Functionalizing agent	Surface area ($m^2 \cdot g^{-1}$)	Sulfur %	Initial [Hg]	pH	q_e	Ref.
BMS Biochar	Poplar Wood Chips	3-MPTS	61.34	0.79	1.0–25 $mg \cdot L^{-1}$	7	320.1 $mg \cdot g^{-1}$	51
SAC	Activated Carbon	Elemental sulfur	764.9	5.75	96 $\mu g \cdot L^{-1}$	8.2	1.87 $mg \cdot g^{-1}$	52
GAC-H_2SO_4 @ 30°C	Activated Carbon	H_2SO_4	620	1.1	1000 $mg \cdot L^{-1}$	7	141.33 $mg \cdot g^{-1}$	53
GAC-H_2SO_4 @ 50°C	Activated Carbon	H_2SO_4	620	1.1	1000 $mg \cdot L^{-1}$	7	151.22 $mg \cdot g^{-1}$	53
ACS	Activated Carbon	3-MPTS	723.87	2.99	5 $mg \cdot L^{-1}$	7	116 $mg \cdot g^{-1}$	54
BCS	Bio Char	3-MPTS	4.24	0.12	5 $mg \cdot L^{-1}$	7	83.2 $mg \cdot g^{-1}$	54
3-MPS-VT	Vermiculite	3-MPTS	129±6	0.98±0.2	21±2 $mg \cdot L^{-1}$	6	286.26 $\mu g \cdot g^{-1}$	55
SA-900	Raw Coal	K_2S	50.0	2.7	24 $mmol \cdot L^{-1}$	–	1.24 $mmol \cdot g^{-1}$	56
Ligsulf-1/2	Lignin Alkali	Sodium Thiocyanate	1413.0	6	10 $mg \cdot L^{-1}$	6	99.98 $mg \cdot g^{-1}$	This Study

second-order, Elovich, and intraparticular kinetic models (**Equations 5–8**, **Table 6**) were used to simulate the interaction of Hg and sulfur functionalized biocarbon. [57–60] Pseudo-second-order model was best fitting (**Figure 5**) for the adsorption data with an R^2 of 0.998, as previous studies about chemisorption were described with a pseudo-second-order model.[52–56] This phenomenon was also noted that the adsorption of Hg was mainly on the surface of the sulfur modified carbon materials.[61] Therefore, introducing heteroatoms such as sulfur will increase the surface polarity enabling the easy ion exchange reactions between mercury and the heteroatoms.[32] Interactions of the chemical nature help explain mercury's affinity towards sulfur forming $Hg(SH)_2$, $Hg_2(SH)_2$, or even $HgSO_4$.[33]

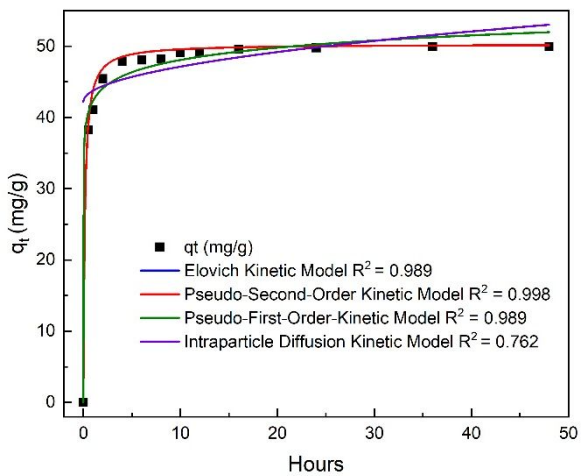

Figure 5. Kinetic curve fitting of Ligsulf-1/2.

In order to study other factors for Hg adsorption, the adsorption kinetic study was done under a pH of 5, 6, and 7. The pH of the solution plays a vital role in mercury adsorption in aqueous solutions. When pH is lower than 2, Hg exists as $Hg^{2+,}$ and at higher pH Hg exists as Hg^{0+} and $Hg(OH)_2$. Higher pH Hg species have a higher affinity for binding sites because of their softer properties as a Lewis Acid.[62] A pH between 7 and 8.2 was used for the adsorption Hg.[51–54,61,63,64] This research showed similar adsorption in pH 7 and 5 compared to pH 6. while a temperature of 25 °C was optimal for mercury adsorption.

The time needed for adsorption and desorption to reach equilibrium is known as equilibrium contact time. It has been studied that for mercury adsorption the uptake is generally fast in the beginning and quickly occupies the vacant functional groups in the adsorbing material.[65] The initial concentration and surface area are key to the equilibrium being reached in batch experiments.[66]

Table 6. Kinetic modeling equations used for the kinetic curve fitting.

Pseudo-first-order	$Log(q_e - q_t) = Log q_e - \frac{k_1}{2.303} t$	*Eq. (5)*
Pseudo-second order	$\frac{t}{q_t} = \frac{1}{k_2 q_e^2} + \frac{t}{q_e}$	*Eq. (6)*
Intraparticle diffusion	$q_t = k_{di}\sqrt{t} + C_i$	*Eq. (7)*
Elovich	$q_t = \frac{1}{\beta}\ln(t) + \frac{t}{\beta}\ln(\alpha\beta)$	*Eq. (8)*

The Hg(II) adsorption and porosity parameters of previous reported sorbents are listed in **Table 5**. Compared to these reported carbon sorbents, Ligsulf-1/2 possesses the highest surface area that possibly the main reason for a fast Hg(II) adsorption rate. The reported sorbents showed a higher q_e with higher initial concentrations[46,48] or a smaller volumes for batch adsorption.[49] Further, the mercury adsorption from aqueous solution was studied applying adsorption isotherms under equilibrium conditions to understand the adsorption process and to determine the adsorption capacity of adsorbent. The adsorption isotherm study of Hg(II) adsorption on Ligsulf-1/2 was conducted by varying the initial concentrations of mercury from 5 $mg \cdot L^{-1}$ to 25 $mg \cdot L^{-1}$, and the final mercury ion concentration was measured using ICP-MS. The experimental data obtained from experiments were fitted to the Langmuir and Freundlich adsorption isotherm models, which are suitable for solid-liquid phase adsorption. The Langmuir adsorption isotherm model based on irreversible monolayer adsorption on a homogenous surface with a finite number of identical adsorbent sites with no adsorbate -adsorbate interaction.

The Freundlich adsorption model, on the other hand, takes into consideration the heterogeneous surface with non-identical adsorption sites.[67] The mathematical expression of these models can be represented as equation (9) and (10).[67]

Langmuir equilibrium adsorption isotherm: $q_e = \left(\frac{q_m * C_e * K_l}{1 + (C_e * K_l)}\right)$ (9)

Freundlich equilibrium adsorption isotherm: $q_e = K_f * C_e^{1/n}$ n>1 (10)

Where q_e is the experimental adsorption capacity (mg·g^{-1}), Ce is the residual equilibrium concentration (mg·L^{-1}) of the mercury ion in the solution, q_m is the maximum adsorption capacity (mg·g^{-1}) of the adsorbate, and K_l is the Langmuir constant, respectively. K_f and n are Freundlich constant and adsorption intensities, respectively. **Figure 6** depicts the observed and fitted mercury adsorption data with Langmuir and Freundlich isotherm models. **Table 7** summarized the isotherm parameters obtained using Langmuir and Freundlich models. The R^2 values revealed that the adsorption of mercury on the Ligsulf-1/2 occurred in monolayer followed, hence, followed the Langmuir isotherm. The maximum adsorption capacity of Ligsulf-1/2 for Hg(II) ions was calculated to be 95.53 mg·g^{-1} by Langmuir isotherm model that was slightly higher than the experimental value (91.5 mg·g^{-1}).

Table 7. Langmuir and Freundlich isotherm parameters for adsorption of Hg(II) ions on Ligsulf-1/2.

Equilibrium model	Parameters	value
Langmuir isotherm	K_l	5.687
	q_m	95.53
	R^2	0.942
Freundlich isotherm	K_f	69.97
	n	5.108
	R^2	0.794

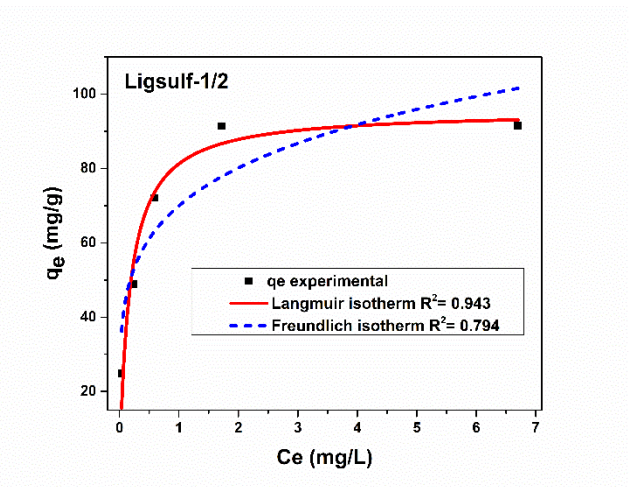

Figure 6: Langmuir and Freundlich adsorption isotherm models for the adsorption of Hg(II) ions onto Ligsulf-1/2. The solid line and dotted line represent the Langmuir and Freundlich fittings to the experimental data, respectively. V = 250 mL, pH = 6, and adsorbate = 50 mg, T = 25 °C.

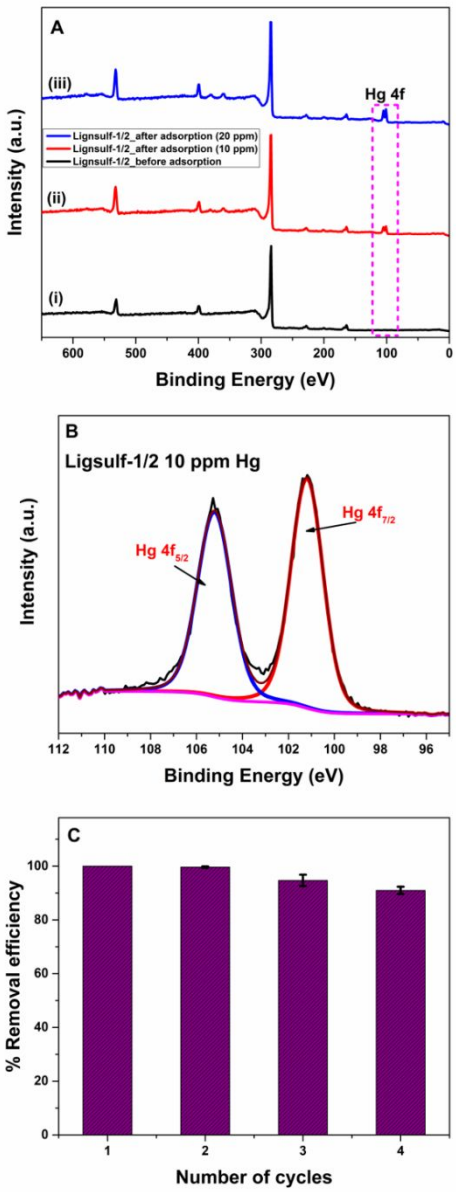

Further, ATR-FTIR (Figure S5,6) and X-ray photoelectron spectroscopy (XPS) of samples before and after adsorption were performed to explore the adsorption mechanism of sulfur-functionalized biocarbon for Hg(II). **Figure 7A** shows the XPS survey spectra of Ligsulf-1/2 before and after adsorption tests with 10 and 20 mg·L^{-1} of Hg(II) solution. Compared to Ligsulf-1/2 biocarbon before adsorption of Hg(II) ions, two peaks appeared at 101.3 and 105.3 eV in 10 and 20 ppm mercury treated biocarbon (**Figure 7B**). These peaks are attributed to the binding energies of Hg $4f_{7/2}$ and Hg $4f_{5/2}$, respectively.[68] The XPS results suggested that the adsorbed mercury remained in its initial oxidation state (+2) after being adsorbed by Ligsulf-1/2. Importantly, no obvious chemical changes, whether involving oxidation or reduction, were identified. These data clearly suggest that the interaction between mercury and the adsorbent was predominantly chemisorptive, driven by electrostatic interaction between positively charged Hg (II) and electron-rich sulfur-containing biocarbon. The strength of the peaks is larger in the 20 ppm treated solution, indicating an increased quantity of mercury on the biocarbon, which was confirmed by the experimental results.

To determine the real-time utility of an adsorbent material, it must be tested for its working performance in the presence of interfering contaminants. We investigated the selective adsorption ability of Ligsulf-1/2 for Hg(II) in binary and ternary solutions. In one experiment, 10 ppm of Na^+ and Ca^{2+} ions were individually added to an aqueous solution of 10 ppm Hg(II) ions. In another experiment, 10 ppm of Na^+ and Ca^{2+} were added simultaneously to 10 ppm of Hg(II) ion solution. We then used ICP-MS to determine the final concentration of Hg(II) ion after treated with Ligsulf-1/2 for 4 hours, 12 hours, and 24 hours, both with and without the presence of interfering ions. The detected mercury concentration in all the samples was found to be below the detection limit of the ICP-MS, which is <0.176 ppb. Results illustrates that Ligsulf-1/2 displayed outstanding selectivity for Hg(II), efficiently removing

Figure 7. XPS survey spectra of Ligsulf-1/2 before and after mercury adsorption (A), High resolution XPS spectra (B) Hg 4f, (C) Regeneration of Ligsulf-1/2 using 0.5M HCl and mercury removal efficiency for successive four cycles.

100% of the Hg(II) from both binary and ternary solutions. These results indicated that Ligsulf-1/2 has a high selectivity and affinity for Hg(II) ions, affirming its potential as an excellent adsorbent material. The desorption of adsorbate and the subsequent regeneration of the adsorbent material are critical elements that considerably impact the cost of any designed adsorption system. To examine the reusability potential of Ligsulf-1/2, we performed four successive absorption-desorption cycles with an initial Hg(II) concentration of 10 ppm and an adsorbent dosage of 0.2 mg/mL. After the first adsorption experiment, Hg-loaded Ligsulf-1/2 was treated for 4 hours in 250 mL of a 0.5 M HCl desorption solution, followed by washing with DI water until a neutral pH was obtained.[69,70] The regenerated Ligsulf-1/2 was then dried at 110°C for 24 hours. Notably, some loss of the adsorbent occurred during the separation and washing procedure, leading to a slight adjustment in the subsequent mercury solution volume while keeping the adsorbent dose constant (0.2 $mg \cdot mL^{-1}$). The adsorption-desorption experiments were conducted for four consecutive cycles, and the mercury removal results are shown in **Figure 7C**. Ligsulf-1/2 displayed outstanding effectiveness in the first two cycles, eliminating approximately 100% of the mercury ion from the solution. However, the mercury adsorption was slightly reduced to 94.2% and 90.7% in the third and fourth cycles, respectively. This decline can be attributed to a gradual decrease in the number of active adsorbent sites accessible in each cycle, possibly as a result of partial desorption. Nonetheless, the fact that the mercury removal remains significant up to the fourth cycle, highlighting the potential of Ligsulf-1/2 as a viable and reusable adsorbent for efficient mercury removal from drinking water and waste water applications.

Conclusions

A series of sulfur dopped biocarbon sorbents were created from low-cost lignin alkali for the purpose of mercury adsorption and environmental remediation. Sodium thiocyanate was used as an activation agent, and a sulfur source, i.e, a dual role for sulfur functionalized biocarbon preparation. Sulfur heteroatoms grafted to activated biocarbon showed superior mercury uptake ability compared to those of pristine non functionalized activated biocarbons. The sorbent denoted Ligsulf-1/2, with 6 % sulfur content, with a mass ratio of 1:2 lignin alkalai to sodim thiocyanate. was synthesized with a surface area of 1413 $m^2 \cdot g^{-1}$ and its counterparts synthesized in the absence of sodium thiocynate have a low surface area (6.2 $m^2 \cdot g^{-1}$). The LigSulf-1/2 showed rapid adsorption kinetics with 97.5% mercury sequestering in the 4 hours. Pseudo second-order fitting showed that adsorption was rate dependent and performed well under a pH of 5 and 7 with a pH of 5 being slightly better. The excellent performance of Ligsulf-1/2 is ascribed to its high surface area and high sulfur dopping, which is achieved simtamioeously by using sodium thiocyanate as an activation agent. The narrow microporous distribution contributed to the increased surface area and the ability for mercury adsorption at low pressure, as seen with the type I isotherm from the N_2 adsorption studies. This work provides a facile method for the preparation of low-cost high, surface area sulfur functionalized biocarbons, which may inspire the exploration of the use of this material for environmental remediation and other potential applications such as energy storage and conversion.

Acknowledgements

This publication was made possible by the National Science Foundation EPSCoR Grant No. 1757353 and the State of Delaware.

Louis Stokes Alliance for Minority Participation - Bridge to the Doctorate Funded by NSF.

XPS analysis was performed with the instrument sponsored by the National Science Foundation under grant No. CHE-1428149.

EM experiments (J.C. and D.K.H.) were conducted at the Center for Nanophase Materials Sciences, which is supported by the U.S. Department of Energy, Office of Science, Basic Energy Sciences, Scientific User Facility Division.

Acknowledgment is made to the Donors of the American Chemical Society Petroleum Research Fund for support of this research.

Notes and references

[a]Department of Chemistry, Delaware State University, Dover, Delaware 19901, United States; E-mail: yyue@desu.edu.

[b]Surface Analysis Facility, University of Delaware, Newark, DE 19716, United States.

[c]Center for Nanophase Materials Sciences, Oak Ridge National Laboratory, Oak Ridge, Tennessee 37831, United States.

[d]College of Materials Science and Engineering, Fuzhou University, Fuzhou, Fujian Province 350108, China; E-mail: guozhy@fzu.edu.cn.

†Electronic Supplementary Information (ESI) available: [raw data behind the associated charts is included]. See DOI: 10.1039/b000000x/

1 K. Xue, Y. Si, S. Xie, J. Yang, Y. Mo, B. Long, W. Wei, P. Cao, H. Wei, H. Guan, E. G. Michaelis, G. Guo, Y. Yue and C. Shan, *Front Chem*, *Front. Chem.*, 2021, **9**, 647545.

2 D. Lv, Q. Wu, D. Ouyang, M. Wen, G. Zhang, S. Wang and L. Duan, *J. Environ. Sci.*, 2023, **123**, 222–234.

3 S. M. Shadman, M. Daneshi, F. Shafiei, M. Azimimehr, M. R. Khorasgani, M. Sadeghian, H. Motaghi and M. A. Mehrgardi, in *Electrochemical Biosensors*, Elsevier, 2019, Chap. 8, 213–251.

4 G. Liu, Y. Cai and N. O'Driscoll, Eds., E*nvironmental Chemistry and Toxicology of Mercury*, John Wiley & Sons, Nashville, TN, 2012.

5 I. R. Hilgendag, H. K. Swanson, C. W. Lewis, A. D. Ehrman and M. Power, *Sci. Total Environ*., 2022, **841**, 156424.

6 A. B. G. Lansdown, *The Carcinogenicity of Metals Issues in Toxicology Series*, 2014.

7 L. Wang, D. Hou, Y. Cao, Y. S. Ok, F. M. G. Tack, J. Rinklebe and D. O'Connor, *Environ Int.*, 2020, **134**, 105281.

8 M.-S. Liao and Q.-E. Zhang, *Theochem*., 1995, **358**, 195–203.

9 M. K. Kim and K. D. Zoh, *J. Prev. Med. Public Health*, 2012, **45**, 335–343.

10 J. D. Demers, J. D. Blum and D. R. Zak, *Global Biogeochem. Cycles*, 2013, **27**, 222–238.

11 R. C. Harris, J. W. M. Rudd, M. Amyot, C. L. Babiarz, K. G. Beaty, P. J. Blanchfield, R. A. Bodaly, B. A. Branfireun, C. C. Gilmour, J. A. Graydon, A. Heyes, H. Hintelmann, J. P. Hurley, C. A. Kelly, D. P. Krabbenhoft, S. E. Lindberg, R. P. Mason, M. J. Paterson, C. L. Podemski, A. Robinson, K. A. Sandilands, G. R. Southworthn, V. L. St. Louis and M. T. Tate, *Proc Natl Acad Sci U S A*, 2007, **104**, 16586–16591.

12 T. W. Clarkson, J. B. Vyas and N. Ballatori, *Am. J. Ind. Med.*, 2007, **50**, 757–764.

13 S. Homma-Takeda, M. Shinyashiki, I. Nakai, C. Tohyama, Y. Kumagai and N. Shimojo, *Anal. Lett.*, 1996, **29**, 601–611.

14 A. C. Bittarello, J. C. S. Vieira, C. P. Braga, I. da Cunha Bataglioli, G. de Oliveira, L. C. Rocha, L. F. Zara, M. A. R. Buzalaf, L. C. S. de Oliveira, J. Adamec and P. de Magalhães Padilha, S*ci. Total Environ*., 2020, **711**, 134547.

15 Z. Yin, H. Jiang, T. Syversen, J. B. T. Rocha, M. Farina and M. Aschner, *J. Neurochem.*, 2008, **107**, 1083–1090.

16 D. Normile, *Science*, 2013, **341**, 1446–1447.

17 J. Wang, X. Feng, C. W. N. Anderson, Y. Xing and L. Shang, *J. Hazard. Mater.*, 2012, **221–222**, 1–18.

18 M. Harada, J. Nakanishi, S. Konuma, K. Ohno, T. Kimura, H. Yamaguchi, K. Tsuruta, T. Kizaki, T. Ookawara and H. Ohno, *Environ. Res.*, 1998, **77**, 160-164.

19 Q. Pu, K. Zhang, A. J. Poulain, J. Liu, R. Zhang, M. A. Abdelhafiz, B. Meng and X. Feng, *J. Hazard. Mater*., 2022, **435**, 129055.

20 R. Jia, J. Zhou, J. Chu, M. Shahbaz, Y. Yang, D. L. Jones, H. Zang, B. S. Razavi and Z. Zeng, *J. Clean Prod.*, 2022, **362**, 132265.

21 T. Wajima, *Process Saf. Environ. Prot.*, 2017, **112**, 342–352.

22 A. Melliti, M. Yılmaz, M. Sillanpää, B. Hamrouni and R. Vurm, *Colloids Surf. A Physicochem. Eng. Asp*., 2023, **672**, 131775.

23 J. Lan, B. Wang, C. Bo, B. Gong and J. Ou, *J. Ind. Eng. Chem*., 2023, **120**, 47–72.

24 M. Mariana, T. Alfatah, H. P. S. Abdul Khalil, E. B. Yahya, N. G. Olaiya, A. Nuryawan, E. M. Mistar, C. K. Abdullah, S. N. Abdulmadjid and H. Ismail, *J. Mater. Res. Technol.*, 2021, **15**, 2287–2316.

25 W. Zhang, X. Qiu, C. Wang, L. Zhong, F. Fu, J. Zhu, Z. Zhang, Y. Qin, D. Yang and C. C. Xu, *Carbon Research,* 2022, **1**, 14.

26 J. R. Rugarabamu, D. Zhao, S. Li, R. Diao and K. Song, *Pet. Res.*, 2023, **8**, 103–117.

27 C. Shan, X. Feng, J. Yang, X. Yang, H. Y. Guan, M. Argueta, X. L. Wu, D. S. Liu, D. J. Austin, P. Nie and Y. Yue, *Carbon*, 2020, **157**, 308–315.

28 I. Neme, G. Gonfa and C. Masi, *Heliyon*, 2022, **8**, e11940.

29 A. E. Vasu, *E-J. Chem*., 2008, **5**, 814–819.

30 C. Shan, Y. Wang, S. Xie, H. Y. Guan, M. Argueta and Y. Yue, *J. Chem. Technol. Biotechnol*., 2019, **94**, 3793–3799.

31 C. Valenzuela, A. Macias, G. A. B. Garcia and V. G. Serrano, *Carbon*, 1990, **28**, 321–335.

32 W. Kiciński, M. Szala and M. Bystrzejewski, *Carbon*, 2014, 68, 1–32.

33 D. Saha, S. Barakat, S. E. Van Bramer, K. A. Nelson, D. K. Hensley and J. Chen, *ACS Appl. Mater. Interfaces*, 2016, **8**, 34132–34142.

34 W. Dong, Y. Bian, L. Liang and B. Gu, *Environ. Sci. Technol.*, 2011, **45**, 3576–3583.

35 M. Svensson, B. Allard and A. Düker, *Sci. Total Environ*., 2006, **368**, 418–423.

36 N. Asasian and T. Kaghazchi, *Int. J. Environ. Sci. Technol*., 2015, **12**, 2511–2522.

37 H. Louie, C. Wong, Y. J. Huang and S. Fredrickson, *Anal. Meth.*, 2012, **4**, 522–529.

38 J. Allibone, E. Fatemian and P. J. Walker, *J. Anal. At. Spectrom.*, 1999, **14**, 235–239.

39 S. Lau, Master Thesis, University of New Hampshire, 2016. Inorganic Ventures, https://www.inorganicventures.com/pub/media/wysiwyg/files/mercury_preservation_techniques.pdf

40 D. E. Dobb, R. C. Metcalf, R. W. Gerlach and L. C. Butler, Proceedings of the I & EC Special Symposium, American Chemical Society, Atlanta, GA, 1994, 1438–1441.

41 B. T. Sturman, *J. Anal. At. Spectrom.*, 2000, **15**, 1512–1512.

42 Z. Liu, F. Zhen, Q. Zhang, X. Qian, W. Li, Y. Sun, L. Zhang and B. Qu, *Bioresour. Technol.*, 2022, **359**, 27471.

43 Q. Qiao, S. Singh, S. L. Lo, V. C. Srivastava, J. Jin, Y. Yu and L. Wang, *J. Taiwan Inst. Chem. Eng.*, 2021, **119**, 204–212.

44 D. A. Khuong, T. T. Kieu, Y. Nakaoka, T. Tsubota, D. Tashima, H. N. Nguyen and D. Tanaka, *Chemosphere*, 2022, **299**, 134365.

45 B. Zhang, S. Petcher, H. Gao, P. Yan, D. Cai, G. Fleming, D. J. Parker, S. Y. Chong and T. Hasell, *J. Colloid Interface Sci.*, 2021, **603**, 728–737.

46 J. H. Park, J. J. Wang, B. Zhou, J. E. R. Mikhael and R. D. DeLaune, *Environ. Pollut.,* 2019, **244**, 627–635.

47 Y. Guo, Z. Zeng, Y. Zhu, Z. Huang, Y. Cui and J. Yang, *Appl. Catal. B*, 2018, **220**, 635–644.

48 S. Liu, Q. Li, S. Zuo and H. Xia, *Microporous Mesoporous Mater*., 2022, **336**, 111876.

49 M. Sevilla, J. Carro-Rodríguez, N. Díez and A. B. Fuertes, *Sci. Rep*., 2020, **10**, 4866.

50 J. Serafin, B. Dziejarski, O. F. Cruz Junior and J. Sreńscek-Nazzal, *Carbon*, 2023, **201**, 633–647.

51 H. Lyu, S. Xia, J. Tang, Y. Zhang, B. Gao and B. Shen, *J. Hazard. Mater.*, 2020, **384**, 121357.

52 C. J. Hsu, Y. H. Chen and H. C. Hsi, *Sci. Total Environ*., 2021, **784**, 147240.

53 N. Asasian Kolur, S. Sharifian and T. Kaghazchi, *Turk. J. Chem.*, 2019, **43**, 663–675.

54 S. Xia, Y. Huang, J. Tang and L. Wang, *Environ. Sci. Pollut. Res. Int*., 2019, **26**, 8709–8720.

55 F. H. do Nascimento, D. M. de Souza Costa and J. C. Masini, *Appl. Clay Sci.*, 2016, **124–125**, 227–235.

56 T. Wajima and K. Sugawara, *Fuel Process. Technol.*, 2011, **92**, 1322–1327.

57 G. Skodras, I. Diamantopoulou, G. Pantoleontos and G. P. Sakellaropoulos, *J. Hazard. Mater.*, 2008, 158, 1–13.

58 K. V. Kumar, *J. Hazard. Mater.*, 2007, **142**, 564–567.

59 I. Feddal, G. Mimanne, A. Dellani and S. Taleb, *Mater. Today,* 2022, **49**, 981–985.

60 R. L. Tseng, H. N. Tran and R. S. Juang, *J. Taiwan Inst. Chem. Eng.*, 2022, **137**, 104294.

61 P. Liu, C. J. Ptacek, K. M. A. Elena, D. W. Blowes, W. D. Gould, Y. Z. Finfrock, A. O. Wang and R. C. Landis, *J. Hazard. Mater.*, 2018, **347**, 114–122.

62 H. Qin, P. He, J. Wu and N. Chen, *Chem. Eng. J.*, 2020, **380**, 122505.

63 K. Chen, Z. Zhang, K. Xia, X. Zhou, Y. Guo and T. Huang, *ACS Omega*, 2019, **4**, 8568–8579.

64 M. A. Al-Ghouti, D. Da'ana, M. Abu-Dieyeh and M. Khraisheh, *Sci. Rep.*, 2019, **9**, 1–15.

65 P. Hadi, M. H. To, C. W. Hui, C. S. K. Lin and G. McKay, *Water Res.*, 2015, **73**, 37–55.

66 K. Anoop Krishnan and T. S. Anirudhan, *J. Hazard. Mater.*, 2002, **92**, 161–183.

67 K. Jahan, V. Singh, N. Mehrotra, K. Rathore and V. Verma, *Biomass Convers. Biorefin.*, 2023, **13**, 6913–6923.

68 Y. Tang, M. Zheng, W. Xue, H. Huang and G. Zhang, *Sep. Purif. Technol*., 2022, **287**, 120577.

69 M. Fayazi, *Environ. Sci. Pollut. Res.*, 2020, **27**, 12270–12279.

70 M. Hadavifar, N. Bahramifar, H. Younesi and Q. Li, *Chem. Eng. J.*, 2014, **237**, 217–228.